Int. J. Multiphase Flow Vol. 17, No. 4, pp. 533–544, 1991
Printed in Great Britain.

0301-9322/91 $3.00 + 0.00

GAS–LIQUID FLOW AT MICROGRAVITY CONDITIONS—I

DISPERSED BUBBLE AND SLUG FLOW

C. COLIN,[1] J. FABRE[1] and A. E. DUKLER[2]

[1]Institut de Mécanique des Fluides, URA CNRS 005, Avenue Camille Soula, 31400 Toulouse, France

[2]Chemical Engineering Department, University of Houston, Houston, TX 77204, U.S.A.

(Received 26 February 1991; in revised form 11 April 1991)

Abstract—Void fraction, pressure gradient and flow pattern data are reported for gas–liquid flow at near-zero gravity through a 4 cm dia tube about 3 m long. These data were collected during a series of parabolic trajectories flown in a jet airplane which provided 15–20 s of reduced gravity at levels $<0.03g$. Flow conditions were such that bubbly or slug flow existed for all runs. High-speed videotapes of the flow were analyzed to obtain the bubble size distribution at two axial locations along the tube. Models for explaining the data are examined.

Key Words: two-phase flow, microgravity, bubble size, flow patterns

INTRODUCTION

The hydrodynamic behavior of a turbulent mixture of gas and liquid flowing through a pipe is strongly influenced by gravity. On Earth, the force of gravity plays a central role in determining the flow pattern, the nature of the coalescence and break up processes of bubbles when they exist, the geometry of the slugs and large Taylor bubbles when flow rates are such that they are observed and on heat and mass transfer rates. The dominant role of gravity becomes clear when it is observed (Taitel & Dukler 1976) that changing the inclination of a pipe carrying gas and liquid from horizontal to $<1°$ upward can change the flow pattern from stratified to slugging. Furthermore, extensive data have shown that, on earth, large changes in surface tension have little influence on the mechanics of the flow. This can be understood by noting that gravitational forces are almost always much greater than interfacial ones. As the gravity level is reduced, a new balance comes into play between inertial and surface forces and as a result the mechanics of the flow can be expected to change. In this paper new data for bubbly and slug flow are presented which were obtained at gravity levels of $<0.03g$. Some interpretations are provided.

The early paper of Hepner *et al.* (1975) gave the first indications that the behavior of gas–liquid systems at low gravity would differ substantially from that at $1g$. Recently, extensive data have been collected at the NASA Lewis Research Center during parabolic flights on a Learjet and in a 100 ft high drop tower (Dukler *et al.* 1988). Drop tower experiments provided 2.2 s of near-zero gravity, for flowing air and water in a pipe of 0.95 cm dia × 46 cm long, while the Learjet gave microgravity sequences 5–8 times longer in experiments carried out in a pipe of 1.25 cm dia × 106 cm long. Flow visualization was obtained using a camera operating at 400 frame/s for Reynolds numbers ranging from 1000 to 12,000 for the liquid and from 100 to 23,000 for the gas. These experiments showed that essentially three characteristic flow patterns existed:

- Bubbly flow at low gas flow rates, where the bubble size is typically smaller than the pipe diameter.
- Slug flow for moderate gas and liquid flow rates, consisting of Taylor bubbles longer than $1D$ and a liquid slug in which smaller bubbles may be dispersed; these bubbles travel axially without significant drift with respect to the Taylor bubbles.
- Annular flow for high gas rates, in which a wavy liquid film exists at the wall on which roll waves propagate.

At conditions where dispersed bubbly flow exists, the bubble size increases monotonically until it occupies a large fraction of the tube cross-sectional area. With further increases, the bubble

lengthens and takes on the appearance of a Taylor bubble with a conical nose and flattened rear. Slug flow is said to exist at the condition where the bubble length exceeds the tube diameter. Thus, it is clear that the transition from bubbly to slug flow is a matter of definition since it does not result from any sudden change in the appearance of the phase distribution with a change in flow rate. This transition appears much more precipitously at 1g. In addition to introducing new data, Dukler *et al.* (1988) suggest physically based models for the transitions between (i) bubbly and slug flow and (ii) slug and annular flow. In the study presented here low-gravity data on flow pattern, voids, bubble size and pressure drop are examined for conditions where the Reynolds numbers are considerably higher than those existing in the Dukler *et al.* (1988) experiments, thus enlarging the magnitude of the inertial forces.

EXPERIMENTAL FACILITY

A schematic diagram of the test facility used for both the ground-based experiments and microgravity conditions during flights is given in figure 1. The test section consists of a transparent plexiglass tube, of 4 cm i.d. × 317 cm long, made up of five parts which are carefully joined. The central part of the tube is 200 cm long. Two windows, each 40.5 cm long, are placed on each side of the central tube. These consist of parallelepipeds made up of transparent plexiglass which surround the test section. The space between the test section and the flat walls is filled with water to minimize distortion of the images taken with high-speed television equipment operating at 500 frame/s. The test section is equipped with two measuring sections placed near the inlet and the outlet, respectively, where pressure taps and the void fraction monitoring equipment are located.

The two phases are supplied through a Venturi mixer. For laboratory experiments the pressure at the outlet is roughly equal to 1 bar, whereas for 0g experiments during flights the pressure inside the plane was kept nearly constant at 0.8 bar. The mixer is a venturi-shaped section with minimum dia 2 cm having eight holes of 1 mm dia located uniformly around the periphery and a divergent length of 25 cm. Water is injected axially while the gas is introduced peripherally.

Air stored in a 50-l. tank under the initial pressure of 200 bar is reduced in pressure to values ranging between 4 and 15 bar depending on the gas flow rate. The outlet of the pressure reducer is connected to one of the three circuits for measuring the gas flow rate, each consisting of a sonic

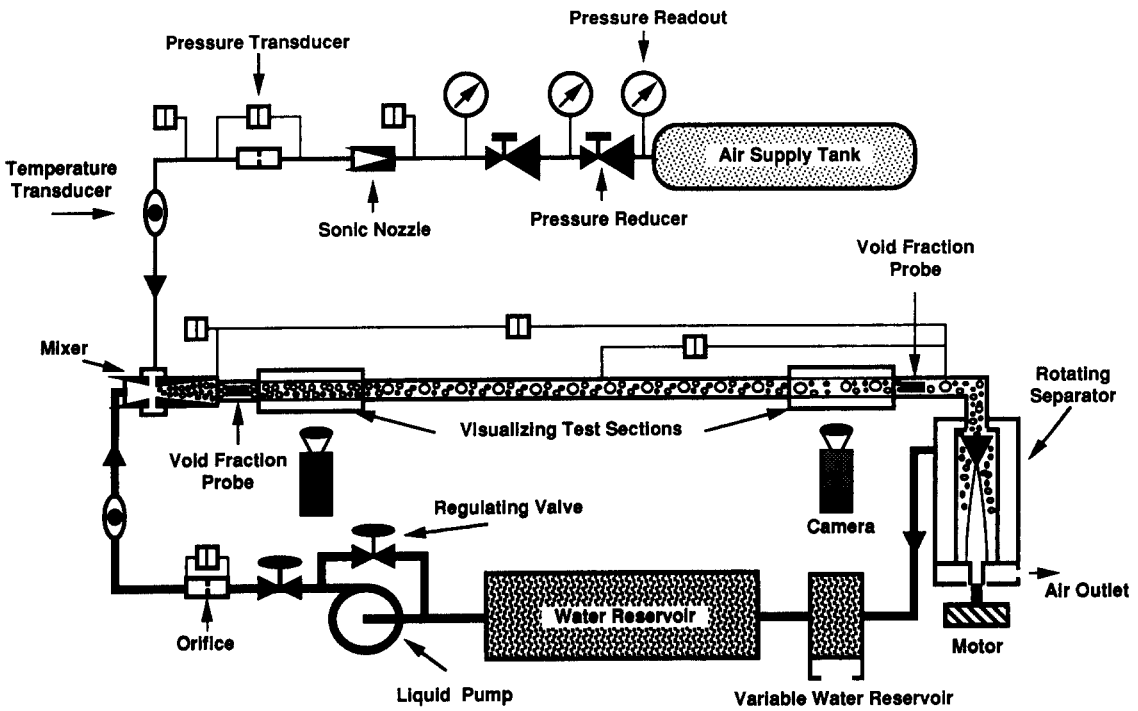

Figure 1. Scheme of the test facility.

nozzle followed by a calibrated orifice plate. The mass flow rate is determined from the absolute pressure upstream of the nozzle as well as from the pressure difference across the orifice. In order to determine the gas density, the temperature as well as the relative pressure inside the pipe are recorded together with the absolute ambient pressure.

Water is stored in a 50-l. reservoir and circulated by a centrifugal pump providing 200 l/min under 1.5 bar. The liquid flow rate is measured with a calibrated orifice plate. Due to the high water demand, it is necessary to recirculate the water during the flights. A rotating gas–liquid separator is located at the outlet of the two-phase flow line. It consists of an external cylinder of 25 cm i.d. × 40 cm high, in which an inner cylinder of 17 cm dia rotates at 1200 rpm. The mixture is injected axially and the liquid is collected by centrifugal force through holes located in the inner cylinder. A variable-volume reservoir is located between the separator and the main water reservoir to compensate for variations of the liquid volume in the system as the flow conditions are changed.

The pressure drop across two lengths of the test section is measured with two pressure transducers. Inlet and outlet void fractions are obtained from conductive probes placed at the measuring stations. Each probe consists of three pairs of electrodes flush-mounted inside the pipe wall with each electrode being a quarter of a cylinder. The main electrodes, of 3 cm height, are placed between secondary guard electrodes of 1 cm height. The electrodes are supplied with alternating current at 10 kHz. The volume of influence of the probes corresponds roughly to a pipe length of $1D$. Careful calibrations in vertical upward flow were carried out for void fractions up to about 0.3 with extrapolation of this calibration used for the few runs having higher void fractions. In order to eliminate the influence of the water temperature and conductivity, reference electrodes are placed in the water supply line.

The data were recorded on a microcomputer hard disk by using a 16-channel A/D converter at sampling frequency of 50 Hz.

EXPERIMENTAL CONDITIONS AT REDUCED GRAVITY

The low-gravity experiments reported here were undertaken in the framework of the French space program (Colin 1990). They were carried out during three series of parabolic flights. During each series 30 parabolic trajectories were performed. During each parabola about 20 s of reduced gravity were available. The experiment was started just after taking off and the flow conditions were changed in the 2-min interval available between two consecutive trajectories. Data were acquired during the approx. 20 s of reduced gravity and the system was checked after every five trajectories for zero drift of the transducers. The component of gravity perpendicular to the floor was recorded continuously using an accelerometer located in the middle of the experimental facility. Its level was in the range $\pm 0.03g$. It is useful to quantify the influence of body force by using dimensionless microgravity numbers. By normalizing the standard deviation of the apparent gravity $\tilde{g}$, defined for each run during the period of experiments, two definitions are useful:

$$Ng_1 = \frac{\Delta\rho \tilde{g} D}{\rho_L U_m^2} \quad \text{and} \quad Ng_2 = \frac{\Delta\rho \tilde{g} D^2}{\sigma},$$

where ρ_L is the liquid density, $\Delta\rho$ is the density difference, D is the pipe diameter, U_m is the mixture velocity and σ is the surface tension. If the gravity level is to be small compared with inertia and surface tension, these two numbers have to be as small as possible. Ng_1 is the inverse of the square of a Froude number, whereas Ng_2 is a Bond number:

$$\mathrm{Fr}_{\mu g} = \frac{1}{\sqrt{Ng_1}} \quad \text{and} \quad \mathrm{Bo}_{\mu g} = Ng_2.$$

The greater $\mathrm{Fr}_{\mu g}$, the better the microgravity quality.

The statistical distribution of the $\mathrm{Fr}_{\mu g}$ values corresponding to 117 runs has been plotted in figure 2. $\mathrm{Fr}_{\mu g}$ ranges between 3 and 37. The runs corresponding to $\mathrm{Fr}_{\mu g} < 5$ have been eliminated due to unacceptable levels of reduced gravity. Visual examination showed that for these cases the flow was not symmetric, as one would expect at microgravity conditions. Thus, increasing the Reynolds number by increasing the pipe diameter in low-gravity experiments requires increasingly lower levels of gravity. For large diameter tubes very low residual gravity levels may not be

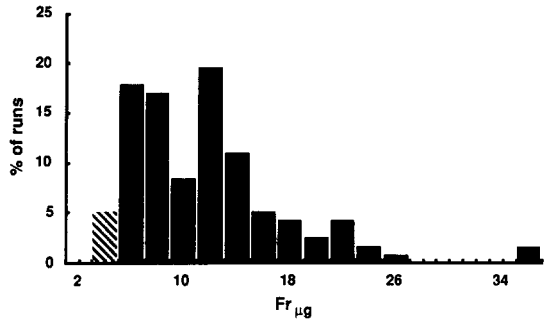

Figure 2. Statistical distribution of $Fr_{\mu g}$.

achievable with parabolic trajectories. The value of $Bo_{\mu g}$ for the best runs was as small as 1.2 and for the worst was as high as 5.6.

TRANSITION BETWEEN BUBBLY AND SLUG FLOW

During each trajectory synchronized 500 frame/s television cameras were used at the windows located just after the mixer and near the exit of the tube. The videotapes thus obtained provided information on the flow pattern at that location and could be analyzed to determine the bubble or slug dimensions and velocities. Results obtained at reduced gravity were compared with those obtained in the laboratory at $1g$ using the same flow loop but with the test section mounted vertically. For these experiments, the mixture Reynolds number, defined as

$$\mathrm{Re}_m = \frac{U_m D}{\nu_L},$$

where ν_L is the liquid viscosity, varied from 10,000 to 80,000. Over this range both bubbly and slug flow could be observed. The flow structure and its changes with flow rate can be described qualitatively as follows:

- At low superficial liquid and gas velocities ($U_{LS} \cong 0.3$ m/s, $U_{GS} \cong 0.1$ m/s), spherical bubbles of a few millimeters appear at the inlet. They coalesce to give larger bubbles of near spherical shape and smaller than $1D$ at the outlet. They travel at near-uniform velocity and are located close to the axis of the tube.
- At higher gas velocities ($U_{LS} \cong 0.3$ m/s, $U_{GS} \cong 0.4$ m/s), coalescence has taken place such that long bubbles having a smooth interface move along the tube separated by nonbubbly liquid slugs.
- At high liquid and low gas velocities ($U_{LS} \cong 1$ to 1.5 m/s, $U_{GS} \cong 0.1$ m/s), dispersed bubbles of a few millimeters diameter are observed. The average bubble size decreases when the liquid flow rate is increased. Coalescence also occurs between the inlet and the outlet of the tube, as evidenced by a difference in bubble size. When the gas flow rate becomes greater the bubble size grows and the interface seems very disturbed. The largest bubbles reach the axis of the tube and coalesce to give bubbles of $1D$ or $2D$ length, the condition of slug flow.
- At higher gas velocities ($U_{Gs} \cong 0.8$ m/s), long bubbles appear having a highly disturbed interface and separated by highly aerated liquid slugs. The liquid film surrounding the elongated bubble becomes thick and may carry small bubbles.

Some individual video frames comparing reduced and normal gravity flows at comparable flow conditions are displayed in figure 3. It is evident that at nearly the same flow conditions the structure is completely different.

The flow patterns have been defined in agreement with the definition of Taitel *et al.* (1980) and Dukler *et al.* (1988). The observations at the outlet section are summarized in the flow pattern map of figure 4. As discussed above, the transition from bubbly to slug flow does not happen suddenly and this can be seen in figure 3, where a frame corresponding to transition condition is included.

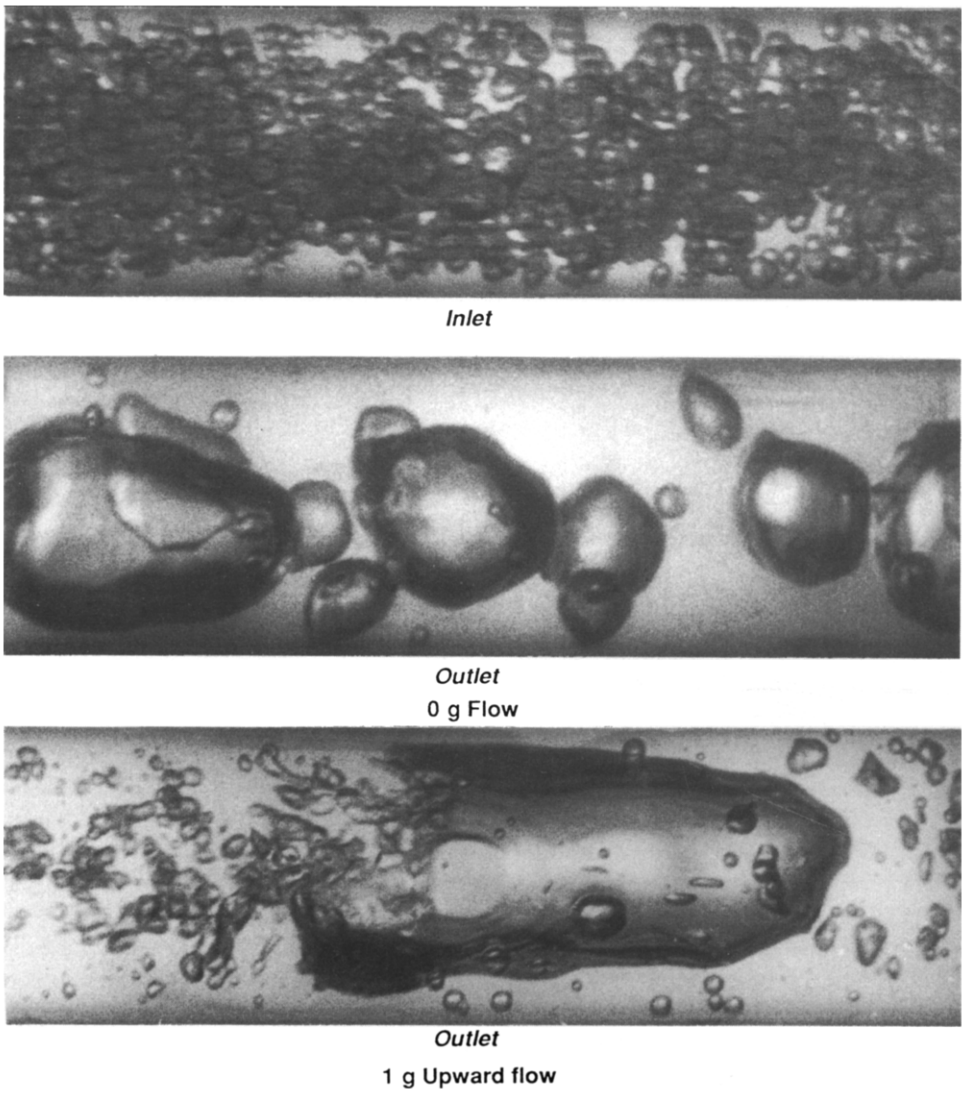

Figure 3. Comparison between inlet and outlet structures, as well as between $0g$ ($U_{LS} = 0.49$ m/s; $U_{GS} = 0.19$ m/s) and $1g$ flow ($U_{LS} = 0.54$ m/s; $U_{GS} = 0.19$ m/s).

By contrast, for vertical upward flow a sudden change in appearance, with a small change in flow rate, in the nature of the bifurcation is observed. Studies of the bubble size distribution discussed below confirm this observation. The experimentally observed transition is represented by the solid line in figure 4, and this is given by the following equation:

$$U_{LS} = 3.2U_{GS}. \quad [1]$$

In the section below, which discusses voids and velocities, it is shown that because the bubbles are located in the center of the tube and are moving with the higher liquid velocity which exists there, the measured bubble axial velocity, $U_G = 1.2U_m$. Since $U_G = U_{GS}/\epsilon$ and $U_m = U_{LS} + U_{GS}$, where U_G is the gas velocity and ϵ is the void fraction, one can find the value of ϵ which generates [1] to be $\epsilon_{crit} = 0.20$. This is the cross-sectional average void fraction at which transition is expected to take place.

Dukler *et al.* (1988) showed that the transition from bubbly to slug flow occurs when the void fraction reaches the critical value of 0.45. This suggests that bubbles of identical size are closely spaced in almost a cubic array with very little gap between adjacent bubbles. Because no significant drift was observed, the resulting transition equation, which agreed well with the data for the lower

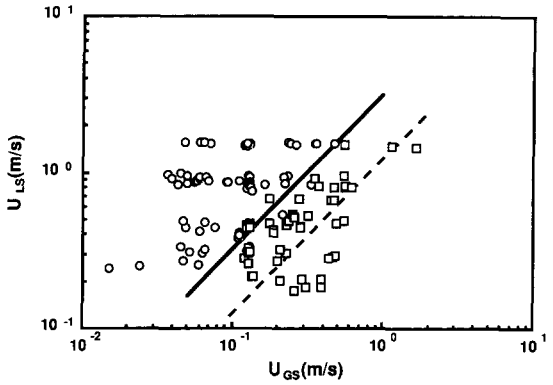

Figure 4. Flow pattern map for the downstream location at 0g conditions: ○, bubbly flow; □, slug flow; ——, [1]; – – –, [2].

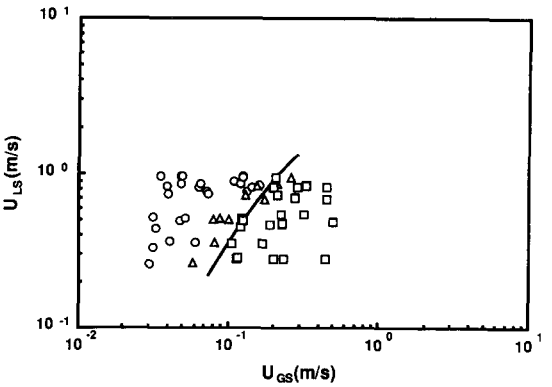

Figure 5. Flow pattern map/1g: ○, bubbly flow; △, transition flow; □, slug flow; ——, [3].

Re_m and smaller diameter tube, was given as

$$U_{LS} = U_{GS}\frac{1-\epsilon_{crit}}{\epsilon_{crit}} = 1.22U_{GS} \qquad [2]$$

and is represented by the dashed line in figure 4.

We speculate that the apparent difference between two predicted voids at which transition takes place for the two different test sections is due to two factors:

(1) In the larger diameter tube used in these experiments the bubbles are located in the central region of the tube, while in the experiments reported by Dukler *et al.* (1988) the bubbles were more uniformly distributed over the cross-section. While the average void fraction at which transition was observed in these experiments was 0.20, the void fraction in the central region where the bubbles existed had to be larger.

(2) Re_m values in the present study ranged from 16,000 to 70,000 at transition, while in the experiments of Dukler *et al.* the upper value was 17,000. Observations of the films show that coalescence is activated by the turbulent motion which induces deformation of the bubble interface. These lateral motions and deformations were much more apparent in the 4 cm tube of the current study than in the 1.27 cm tube of the earlier one, and are undoubtedly due to the higher turbulence levels at the higher Re_m. Also, bubbles which are initially further apart in the larger diameter test section can be expected to collide when driven by the higher turbulence levels and transition can take place at lower voids.

It is of some interest to observe the differences which exist in the bubble to slug transition data for a vertical test section at 1g. Earth gravity results are given in figure 5. In this case, the model must include the rise velocity of the bubbles due to buoyancy. A void fraction at transition of 0.13 gives the following equation, which is represented by the solid curve in figure 5:

$$U_{LS} = U_{GS}\left(\frac{1}{1.2\epsilon_{crit}} - 1\right) - \frac{0.35\sqrt{gD}}{1.2} = 5.41U_{GS} - 0.18. \qquad [3]$$

This transition value of void fraction is small compared with the values near 0.25 obtained by others in vertical upward flow experiments; see, for example, Taitel *et al.* (1980). As reported by these authors, coalescence is rarely observed for $\epsilon < 0.20$. In addition, they claim that using fluids having air and water properties, bubbly flow cannot exist at low liquid velocities in tubes shorter than about 4.5 cm. This prediction results from the fact that small bubbles must overtake Taylor bubbles in such geometries. The present results do not confirm the theory, although it is qualitatively acknowledged that slug flow is more readily formed in small diameter pipes. It would appear that, at least for short tubes of the length used here, the method of gas injection does affect the flow pattern transition, as shown by Clark & Flemer (1985).

The difference in the transitional void fraction between 1g ($\epsilon_{crit} = 0.13$) and reduced gravity ($\epsilon_{crit} = 0.20$) is surprising in view of the fact that more collisions are observed at reduced gravity than are seen to exist at 1g. In vertical upward flow in the laboratory the work done by bubble drift against the interfacial shear stress increases the turbulent dissipation and therefore the turbulence energy of the liquid phase. As a consequence, it would be expected that coalescence is prevented, requiring a higher value of the void fraction at which transition could take place. However, it is observed that at microgravity bubbles may coalesce whatever their size: the bubbles grow monotonously. At 1g bubbles of near equal diameter are less likely to coalesce but the efficient collisions are those of small bubbles entering the wake of the spherical cap bubbles which are rising relative to the surrounding liquid due to gravity: large Taylor bubbles are formed while a population of small millimetric bubbles is maintained. Therefore, fewer collisions are necessary to obtain slug flow in 1g upflow than in 0g conditions and transition occurs for a smaller void fraction. This conclusion is in complete agreement with the results of Dukler *et al.* (1988).

VOID FRACTION AND PRESSURE DROP

Values of the cross-sectional average void fraction, ϵ, were obtained from the conductance probes while the gas velocity, U_G, was determined from the video films by measuring the rate of advance axially of the bubbles. For each run the measured value of the gas velocity was compared with the one calculated from $U_G = U_{GS}/\epsilon$. In most cases these two values were in good agreement. Where they were not, the difference was ascribed to an error in the input gas rate measurement and the data of that run rejected. Data were collected during microgravity trajectories as well as for the vertical tube at 1g. The *in situ* gas velocity is plotted vs mixture velocity in figure 6 for slug flow and in figure 7 for bubbly flow, with the data for microgravity conditions and 1g included. A method widely used to model such data is of the form

$$U_G = C_0 U_m + U_\infty,$$

where U_∞ is the drift velocity of the gas relative to the liquid and C_0 characterizes the relation between local void and velocity distributions (Zuber & Findlay 1965). In vertical upward slug flow, the gas is mainly carried in Taylor bubbles whose velocity is given by the classical law of Nicklin *et al.* (1962):

$$U_G = 1.2U_m + 0.35\sqrt{\frac{\Delta\rho g D}{\rho_L}}. \qquad [4]$$

That the coefficient, $C_0 = 1.2$ in this case is thought to reflect the fact that for turbulent flow in the central region of the tube the velocity of the liquid ahead of the bubble is about 1.2 times that of the mean. This equation is plotted in figure 6 as the dashed line and can be seen to be in good agreement with the measurements. For bubbly flow in vertical tubes the drift of small bubbles has

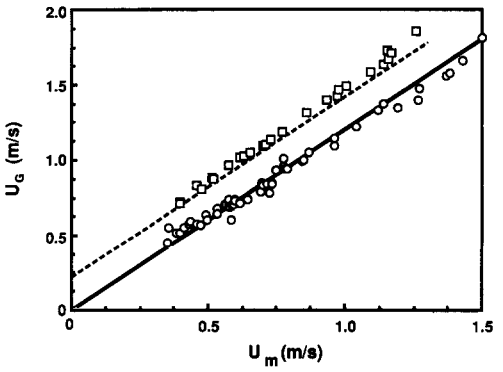

Figure 6. Gas drift in slug flow vs mixture velocity: ○, 0g flow; □, 1g flow; ——, [6]; – – –, [4].

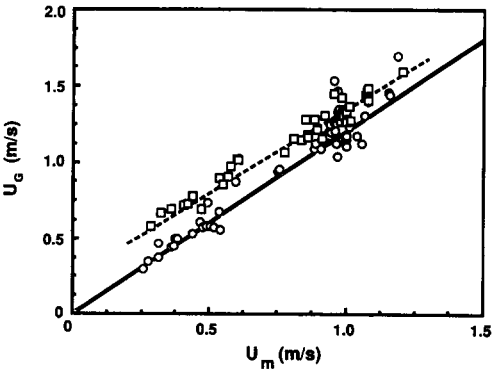

Figure 7. Gas drift in bubbly flow vs mixture velocity: ○, 0g flow; □, 1g flow; ——, [6]; – – –, [5].

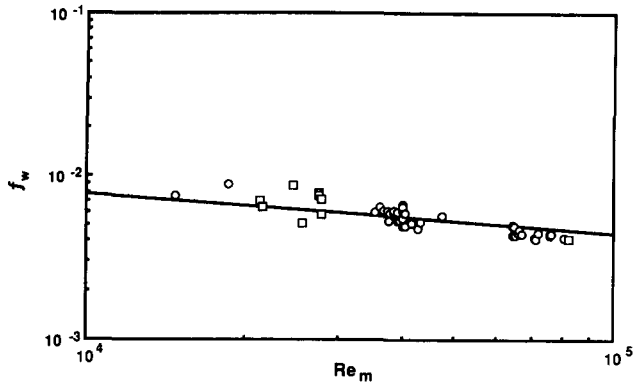

Figure 8. Friction factor vs Re_m in 0g flow: ○, bubbly flow; □, slug flow; ——, [8].

been analyzed by Harmathy (1960) and is given by the second term in the following equation (Zuber & Findlay 1965):

$$U_G = C_0 U_m + 1.53 \left(\frac{\Delta \rho g \sigma}{\rho_L^2} \right)^{0.25}. \quad [5]$$

This equation is plotted as the dashed line in figure 7, where the value $C_0 = 1.1$ gives the best agreement with the data.

In contrast, for microgravity conditions, the gas velocity for both bubbly and slug flow is predicted by setting the relative velocity to zero. For turbulent flow the predicted relationship would then be

$$U_G = 1.2 U_m. \quad [6]$$

Note that even when gravity is suppressed, there remains a drift between the gas and the liquid because the gas bubbles are located in the central region of the pipe and there exists a slow-moving layer near the wall in which there is no gas. This drift does not appear to be sensitive to the flow pattern.

Pressure drop values were validated by comparing the gradients calculated from the two pressure transducers (figure 1). Only the runs for which the two values agreed with 10% were retained for the determination of the friction factor at the wall:

$$f_w = \frac{1}{2} \frac{D \left| \frac{dP}{dx} \right|}{\rho_m U_m^2}, \quad [7]$$

where ρ_m is the mixture density. The results for bubbly and slug flows are plotted vs Re_m in figure 8. They are in good agreement with the Blasius correlation:

$$f_w = 0.079 Re_m^{-0.25}. \quad [8]$$

The reduced gravity bubbly and slug flow data collected here appear to behave as a homogeneous fluid having the density of the mixture and the viscosity of the liquid and moving at the mixture velocity.

These results suggest that it should be possible to model both bubbly and slug flow (at least for conditions far from the slug to annular transition) by a single model with no need to discriminate bubbly from slug flow. The average void fraction and wall shear stress are indistinguishable. However, local void fraction distributions will differ and this will probably make it necessary to apply different approaches to the modeling of heat and mass transfer processes.

BUBBLE SIZE

In order to understand the mechanisms which control the flow pattern, and to understand bubbly flow in more detail, the evolution of bubble size between the inlet and the outlet of the pipe was studied. Single frames from the two video cameras were analyzed to determine the bubble size

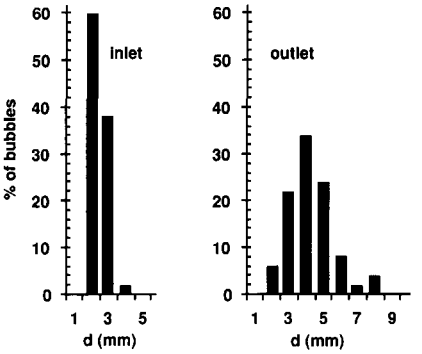

Figure 9. Bubble size distribution in 0g flow: $U_{LS} = 1.56$ m/s; $U_{GS} = 0.06$ m/s.

distribution. The diameter d of each bubble was calculated from the longitudinal and transverse diameters d_x and d_y:

$$d = \sqrt[3]{d_x d_y^2}.$$

The measurements of d_x and d_y were made on a video monitor after calibrating the screen coordinates by using a spherical body placed inside the tube filled with liquid. For most of the results given here the statistic was made with 100 bubbles.

Three examples of the results are given in figures 9–11 for flow conditions corresponding to bubbly flow. The runs of figures 9 and 10 were carried out at reduced gravity with the same gas flow rate and different liquid flow rates. The bubble size distribution at the inlet is essentially the same for the two experiments but at the outlet the bubble size distribution is different. In every case measured the comparison between the inlet and outlet size distributions suggests strongly that coalescence is taking place at a substantial rate along the 80D length between the point of formation and the outlet location. The rate of coalescence appears greater for the run shown in figure 10, this is to be expected in view of the higher void fraction for that run.

A rather drastic difference from these results was noted by Janicot (1988) using the equipment described by Dukler *et al.* (1988). He repeated a series of experiments at reduced gravity in the Learjet with the 1.27 cm dia tube for which films were available at the outlet. In these new runs the flow just downstream of the mixer was filmed. No attempt was made to measure the bubble sizes, but in this smaller diameter tube for most conditions of bubbly flow there appeared to be little difference in the sizes and concentrations of bubbles between the mixer and outlet locations. It would appear that the smaller tube, the lower Re_m and the damped turbulence levels which result suppresses coalescence.

The influence of gravity may be understood by comparing the results of figures 10 and 11 corresponding to the same flow conditions. In vertical flow (figure 11), the bubble distribution does not evolve significantly between the inlet and outlet, indicating that coalescence between small bubbles is suppressed at 1g .

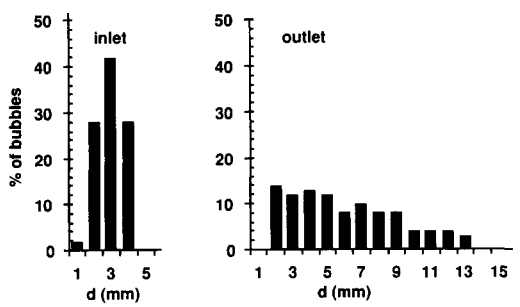

Figure 10. Bubble size distribution in 0g flow: $U_{LS} = 0.85$ m/s; $U_{GS} = 0.05$ m/s.

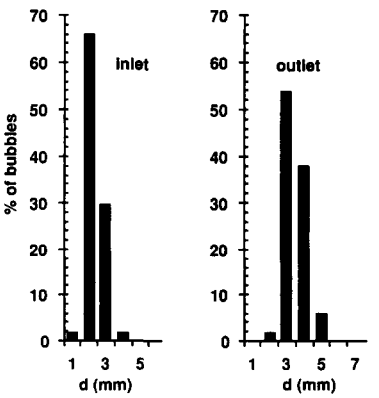

Figure 11. Bubble size distribution in 1g flow: $U_{LS} = 0.86$ m/s; $U_{GS} = 0.05$ m/s.

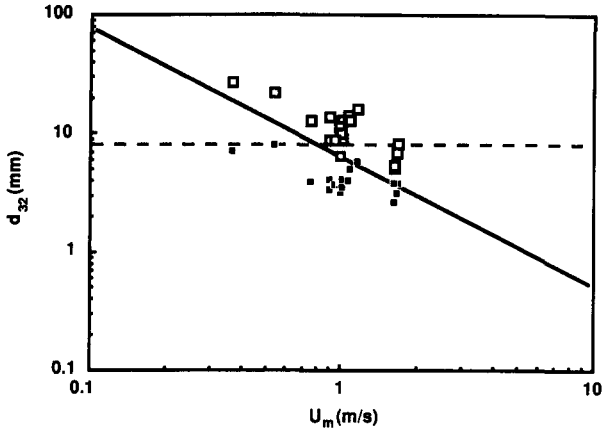

Figure 12. Sauter diameter at the inlet (■) and outlet (□) in 0g flow compared with Hinze's theory; ——, [9].

The Sauter mean diameter was computed from the distributions by

$$d_{32} = \frac{\sum_{i=1,N} d_i^3}{\sum_{i=1,N} d_i^2},$$

where d_i is the diameter of the ith bubble and N is the number of bubbles over which the average was taken. Sauter mean diameters at the inlet and outlet, as calculated from the size distributions for each run, are plotted vs the mixture velocity in figure 12. It is evident that the bubble size increases systematically along the tube axis, confirming the dominant role of coalescence as well as the probable absence of breakup. It is of interest to compare these results with the prediction of the existing theory of breakup.

The breakup theory for dispersions by Hinze (1955) was proposed initially for the emulsification of a liquid in a turbulent flow of another liquid. He assumed that the dynamic pressure fluctuations due to the eddy motion determined the size of the largest drops. Thus, provided the Kolmogorov energy distribution law is valid, the critical diameter above which breakup occurs is given by

$$d_{\text{crit}} = 0.725 \left(\frac{\sigma}{\rho_L}\right)^{3/5} \mathscr{E}^{-2/5} \qquad [9]$$

where $\mathscr{E}$ is the turbulent energy dissipation per unit mass and ρ_L is the liquid density. Sevik & Park (1973) theoretically derived a coefficient with a value of 1.15 for bubble breakup and confirmed its validity by experiment. d_{crit} May be considered the maximum stable bubble size. From d_{crit} and the general shape of the size distribution the values of d_{32} can be computed. In order to apply the theory to pipe flow, the energy dissipation must be estimated. For fully developed single-phase flow, the total energy dissipation balances the internal work of pressure forces. The total dissipation by unit mass averaged over the pipe cross-section $\langle \mathscr{E}_t \rangle$ may be calculated from kinetic energy budget:

$$\langle \mathscr{E}_t \rangle = 2 f_w \frac{U_m^3}{D}.$$

Equation [9] with a coefficient of 1.15 was used to calculate d_{crit} and d_{32}, the Sauter mean diameter. The predicted value of d_{32} was computed from the predicted d_{crit} value using the experimentally measured ratio of d_{32}/d_{crit}, which equals 0.77. Predicted values of d_{32} are shown as the solid line in figure 12. Unexpectedly, the computed values are in satisfactory agreement with the measured bubble sizes at the inlet but substantially underpredict the values further downstream where coalescence has taken place.

The physical reasons for this discrepancy between theory and data remain to be determined. However, extensive study of the videotapes suggests that the absence of drift between the bubbles and the surrounding liquid suppresses eddy shedding from the bubbles and this, in some way,

enhances coalescence but hinders the breakup process. Further studies of this phenomenon are now underway.

CONCLUSION

The results reported here for air–water flow at reduced gravity in a 4 cm dia tube compared with information published earlier for the same system in a 1.27 cm dia tube provide data over a wide range of Reynolds numbers.

A simple form of the drift flux relation can be used to predict the cross-sectional average void fraction for bubbly and slug flow near transition. This is the case, even though there is no relative velocity locally between the bubbles and liquid because most of the bubbles are located in the central region of the pipe. As a result their velocity is higher than the average velocity of the liquid.

For bubbly or slug flow near transition the wall friction can be reasonably estimated using a homogeneous model having the viscosity of the liquid and the mixture density computed from the average void fraction.

The average void fraction at which transition takes place between bubbly and slug flow is influenced by the tube diameter. This is a direct result of the higher turbulence level in the larger tube. As a result, the equation predicting this transition for the 1.27 cm dia test section differs from the one for the new data presented here. It will be necessary to develop data on void distribution in order to generalize this model for all tube sizes.

Measurements of bubble size distributions at inlet and outlet locations show that there is a high rate of coalescence as the fluid flows down the tube. This is in contrast to observations made in the 1.27 cm dia tube, where it was shown to be small. It is concluded that the higher turbulence levels in the large tube play a role. Sauter mean diameters computed from these distribution are considerably higher than those predicted by the Hinze breakup model. It is suggested that the absence of eddy shedding from the back of the bubble somehow enhances coalescence and suppresses the breakup process.

Acknowledgements—This work has been supported by the "Centre National d'Etudes Spatiales" as part of the French space programs. It was strengthened by the cooperation program with the "Lewis Research Center of NASA" and the "Chemical Engineering Department of the University of Houston". The parabolic flights were undertaken with the aircraft "ZERO G" of the "Centre d'Essais en Vol": two campaigns have been supported by the "Centre National d'Etudes Spatiales"; one by the "European Space Agency".

REFERENCES

CLARK, N. N. & FLEMER, R. L. C. 1985 The bubble to slug flow transition in gas–liquid upflow and downflow. *J. Pipelines* **5,** 53–65.

COLIN, C. 1990 Ecoulements diphasiques à bulles et à poches en micropesanteur. Thèse, Institut National Polytechnique de Toulouse.

DUKLER, A. E., FABRE, J. A., MCQUILLEN, J. B. & VERNON, R. 1988 Gas–liquid flow at microgravity conditions: flow pattern and their transitions. *Int. J. Multiphase Flow* **14,** 389–400.

HARMATHY, T. 1960 Velocity of large drops and bubbles in media of infinite and of restricted extent. *AIChE Jl* **6,** 281–288.

HEPNER, D. B., KING, C. D. & LITTLES, J. W. 1975 Zero-gravity experiments in two-phase fluids flow patterns. Presented at the *ICES Conf.*, San Francisco, Calif., ASME Paper TS-ENAs-24.

HINZE, J. O. 1955 Fundamentals of the hydrodynamic mechanism of splitting in dispersion processes. *AIChE Jl* **1,** 289–295.

JANICOT, A. 1988 Studies of gas–liquid flow under reduced gravity conditions. M.Sc. Thesis, Univ. of Houston, Tex.

NICKLIN, D. J., WILKES, J. O. & DAVIDSON, J. F. 1962 Two-phase flow in vertical tubes. *Trans. Instn Chem. Engrs* **40,** 61–68.

SEVIK, M. & PARK, S. H. 1973 The splitting of drops and bubbles by turbulent fluid flow. *Trans. ASME J. Fluids Engng* **95,** 53–60.

TAITEL, Y. & DUKLER, A. E. 1976 A model for predicting flow regime transitions in horizontal and near horizontal gas–liquid flow. *AIChE Jl* **22,** 47–55.

TAITEL, Y., BARNEA, D. & DUKLER, A. E. 1980 Modelling flow pattern transitions for steady upward gas–liquid flow in vertical tubes. *AIChE Jl* **26,** 345–354.

ZUBER, N. & FINDLAY, J. A. 1965 Average volumetric concentration in two phase flow systems. *Trans. ASME J. Heat Transfer* **87,** 453–468.